

Further Investigation of Synaptic Vesicle Protein 2A (SV2A) Ligands Designed for Positron Emission Tomography and Single-Photon Emission Computed Tomography Imaging: Synthesis and Structure–Activity Relationship of Substituted Pyridinylmethyl-4-(3,5-difluorophenyl)pyrrolidin-2-ones

Richard Pracitto, Kyle C. Wilcox, Marcel Lindemann, Jie Tong, Chao Zheng, Songye Li,* Sjoerd J. Finnema, Yiyun Huang, and Zhengxin Cai*

Cite This: *ACS Omega* 2021, 6, 27676–27683

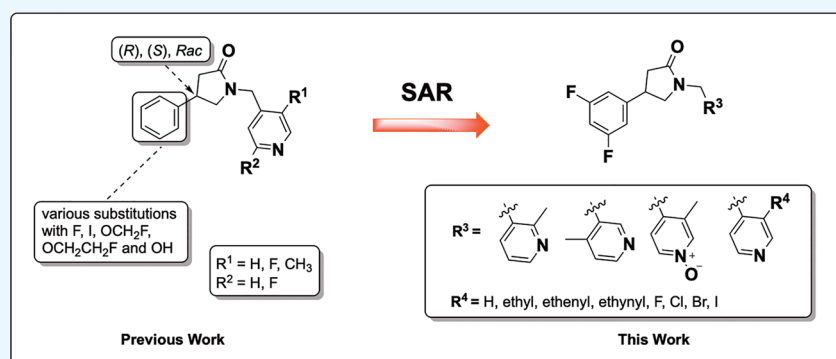
Read Online

ACCESS |

Metrics & More

Article Recommendations

Supporting Information



ABSTRACT: A series of synaptic vesicle protein 2A (SV2A) ligands were synthesized to explore the structure–activity relationship and to help further investigate a hydrogen bonding pharmacophore hypothesis. Racemic SynVesT-1 was used as a lead compound to explore the replacement of the 3-methyl group on the pyridinyl moiety with halogens and hydrocarbons. Pyridinyl isomers of racemic SynVesT-1 were also investigated. Highly potent analogs were discovered including a 3-iodo pyridinyl ligand amenable to investigation as a PET or SPECT imaging agent.

1. INTRODUCTION

Synapse abnormalities are associated with many neuropsychiatric disorders including schizophrenia and Alzheimer's disease amongst others.^{1,2} Synaptic vesicles (SVs) are small, electron-lucent vesicles that are produced and clustered at presynaptic terminals. They are responsible for the storage and release of neurotransmitters and are regenerated pending calcium-triggered exocytosis. SV2 proteins are 12-transmembrane glycoproteins present on the synaptic vesicles of neural cells and part of the large and broadly distributed major facilitator superfamily (MFS). SV2 consists of three isoforms: SV2A, SV2B, and SV2C.³ Only SV2A is ubiquitously expressed in essentially all presynaptic vesicles. This favors its use as a biomarker for synaptic density among other expressed proteins at the presynaptic proteome and synaptic vesicles.¹ The anti-epileptics levetiracetam and brivaracetam target SV2A, and levetiracetam has been used as the lead structure in the rational design of the first series of potent SV2A ligands, UCB-A, UCB-H, and UCB-J, as candidates for radioligand development for positron emission tomography (PET).³

The potent and selective fluoro-substituted 4-phenyl-2-pyrrolidinone derivatives (Figure 1) have proven to be important in the area of SV2A PET imaging as synaptic density probes, with [¹¹C]UCB-J being the most advanced in this series and applied in clinical neuroimaging studies of epilepsy,⁴ AD,⁵ PD,⁶ depression,⁷ and schizophrenia.^{8,9} However, as this class of compounds evolves, some deficiencies have emerged in human trials. For example, [¹¹C]UCB-A has slow binding kinetics and [¹⁸F]UCB-H has a relatively low specific binding signal.^{10–12} Therefore, these PET tracers have significant limitations for imaging and quantifying SV2A in human brain. Ongoing evaluation of mono- and di-fluorinated analogs of UCB-J then

Received: May 8, 2021

Accepted: September 22, 2021

Published: October 8, 2021



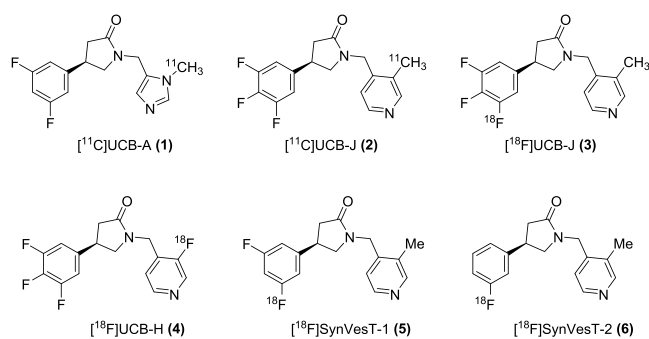


Figure 1. Current SV2A PET imaging probes in this series.

led to the discovery of the novel ^{18}F -labeled SV2A PET tracers [^{18}F]SynVesT-1 (previously known as [^{18}F]SDM-8 or [^{18}F]MNI-1126) and [^{18}F]SynVesT-2 (also known as [^{18}F]SDM-2) (Figure 1), which are currently under first-in-human investigation.^{13,14}

Early efforts toward the discovery of SV2A ligands ultimately lead to the PET tracers shown in Figure 1 including those of Kenda *et al.*¹⁵ and Mercier *et al.*³ In the absence of available structural information on SV2A, ligand-based drug design, further supported by discovery medicinal chemistry efforts, has been used by Mercier *et al.*³ to further define a plausible SV2A pharmacophore. This work led to the hypothesis of a pharmacophore with two hydrogen bond acceptors, one represented by the carbonyl of the pyrrolidinone and the other by the nitrogen of its heterocycle, in particular, imidazole, pyrazole, or pyridine. This produced a series of compounds with dramatically increased SV2A binding affinities.

More recently and specifically aimed at developing fluorine-18-labeled SV2A PET imaging agents, we and others conducted studies to investigate whether structural analogs of UCB-J had suitable binding affinities.¹⁶ These studies focused primarily on the variation of the phenyl substituents of the 4-phenylpyrrolidin-2-one portion of the molecule (Figure 2). Analog

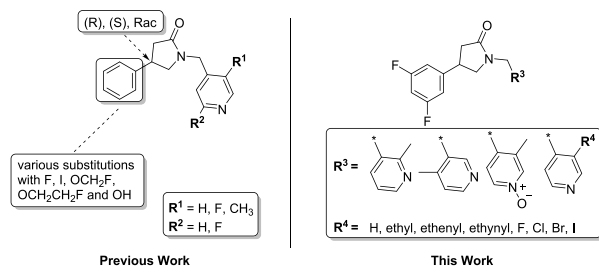


Figure 2. Comparison of this work with previous SAR studies.

screening identified racemic SynVesT-1 (18, 5.1 nM¹⁶ (4.9 nM in our assays)) as having comparable binding affinities with racemic UCB-J. [^{18}F]SynVesT-1 (5) has demonstrated *in vivo* uptake and accumulation in the human brain with favorable kinetics.¹³ In addition, studies revealed sensitivity of SV2A binding to modifications at the 1-(pyridin-4-ylmethyl) portion of other 4-phenylpyrrolidin-2-one variants, i.e., UCB-H and SDM-1.¹⁶ These outcomes presented an opportunity for further SAR studies at the pyridinyl portion of the SynVesT-1 molecule.

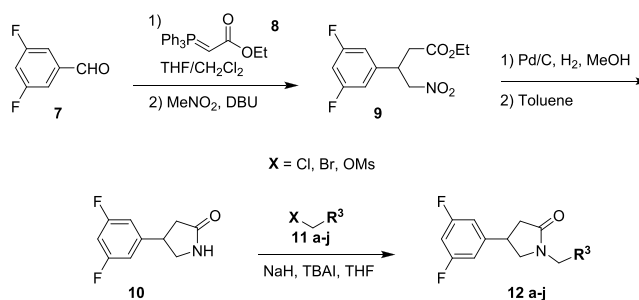
With this background in mind, we set out to explore potential changes in binding affinity (K_i) by modifying the pyridinyl moiety of racemic SynVesT-1 (18). We synthesized a series of compounds according to the following: (1) replacement of the

pyridinyl 3-methyl group with halogens or hydrocarbons and (2) changes in the location of nitrogen on the pyridinyl moiety. We also oxidized the pyridinyl nitrogen of racemic SynVesT-1 (Figure 2). The results of this SAR study may provide further insights into the abovementioned pharmacophore hypothesis.

2. RESULTS AND DISCUSSION

Analogs were prepared using previously reported methods as shown in Scheme 1.¹³ Starting from commercially available 3,5-

Scheme 1. Primary Synthetic Route to Compounds in This SAR Series



fluorobenzaldehyde (7), the Wittig reaction with (carbethoxymethylene)triphenylphosphorane (8) followed by treatment with nitromethane under basic conditions led to compound 9 in 83% yield, which was reduced and cyclized to yield pyrrolidinone 10 in 34% yield. *N*-Alkylation of 10 with various 2- or 3-substituted pyridin-4-ylmethyl halogens or mesylates (11a–j) generated the compounds represented by 12a–j in 5–80% yield.

The *in vitro* binding affinity of these compounds was then tested through competition binding assays with [^3H]UCB-J in human brain tissue homogenates (Table 1; Figure SI-14).

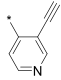
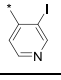
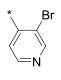
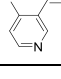
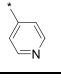
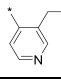
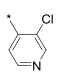
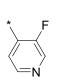
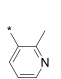
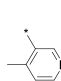
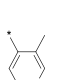
Structure–activity relationships among the compounds evaluated in this study are discussed below.

2.1. Position and Oxidation of the Pyridinyl Nitrogen.

In general, changing the 3-methyl-pyridinyl group of racemic SynVesT-1 (18, 4.9 nM) to a 2-methyl- or 4-methyl-pyridinyl group shows a reduction in affinity, with the 2-methyl isomer (12i, 29.9 nM) having higher affinity than the 4-methyl isomer (12j, 291 nM). These results support a previously reported model consistent with the pyridine nitrogen acting as a hydrogen bond acceptor.³ Studies suggest that the hydrogen bond accepting ability of each pyridinyl nitrogen (2-, 3-, or 4-methylpyridinyl) when compared to each other should not be dramatically different.¹⁷ Therefore, although π interactions may also have influence, the notable differences in potency across these methyl-pyridinyl isomers points to the importance of the nitrogen location as a hydrogen bond acceptor when interacting with SV2A.

The pyridinyl *N*-oxide was the major radiometabolite for pyridinyl-derived SV2A radioligands (2⁹ and 4¹⁸), and we found that the oxidation of the pyridinyl nitrogen shows virtually a complete loss of affinity (12k, 2.8 μM). Although more experimental data are necessary to establish a broader understanding of the effect of pyridine-*N*-oxides across this particular series, it has been experimentally determined previously^{17,19} that in general, pyridine-*N*-oxides are excellent hydrogen bond acceptors and their H-bonding abilities can be influenced by substitution patterns on the pyridine ring (more so than pyridine). *N*-Oxidation also accounts for a marked

Table 1. Binding Data

Compound	R ³	K _i (hSV2A, nM)
12a		4.8 ^a
12b		5.1
12c		5.7
12d		6.2 ^b
12e		6.3 ^a
12f		8.5
12g		13.9
12h		23.0
12i		29.9
12j		291
12k		2772
(13) UCB-A		1.2
(14) UCB-J		2.6 ^a
(15) SynVesT-1		3.1
(16) UCB-H		6.8
(17) SynVesT-2		9.6
(18) Racemic SynVesT-1		4.9 (5.1 ^c)

^an = 2. ^bIt must be noted that while the K_i values for 12a and 12f are statistically different, the intermediate K_i for 12d cannot necessarily be distinguished from either using our current data. ^cPatel *et al.*¹⁶

decrease in lipophilicity by comparison with corresponding pyridines,¹⁷ and differences between the π -electronic structures of pyridine vs pyridine-*N*-oxide are known.²⁰ One might also take into account the bond length of the *N*-oxide, which could be contributing to this loss in affinity.

2.2. The Effect of Hydrocarbons. Removal of the 3-methyl group on the pyridinylmethyl moiety of racemic SynVesT-1 (18, 4.9 nM) showed no improvement in affinity (12e, 6.3 nM (avg, n = 2)). This appears to be consistent with results from previous studies in the 3,4,5-trifluorophenyl pyrrolidinone series.³ Replacing the methyl group with hydrocarbons containing two carbon units of different hybridizations (ethynyl, ethenyl, and ethyl) resulted in a clear affinity trend. The ethynyl (sp¹) derivative was the most potent (12a, 4.8 nM (avg, n = 2)), followed by ethenyl (sp², 12d, 6.2 nM), and ethyl (sp³, 12f, 8.5 nM) (see footnote b, Table 1.). This set of compounds also shows a trend with respect to Hammett constants.²¹ The σ_m constants show a reduction in electron withdrawing potential from ethynyl ($\sigma_m = 0.21$) to ethenyl ($\sigma_m = 0.06$) and slight electron donating potential for ethyl ($\sigma_m = -0.07$). This trend seems to contradict the hypothesis of hydrogen bond basicity at the pyridinyl nitrogen.¹⁷ One might envision the opposite trend, where increased electron withdrawing potential would result in weaker hydrogen bonding, thus reducing the potency across the series.

2.3. The Effect of Halogens. Substitution of the pyridinyl 3-methyl group on racemic SynVesT-1 with halogens resulted in a clear trend with respect to affinity. Substitution with iodine and bromine delivered the most potent compounds in the halogen series 12b (5.1 nM) and 12c (5.7 nM), respectively, whereas chlorine and fluorine substitution led to lower affinities: 14 nM for 12g and 23 nM for 12h, respectively. The observed trend appears to be synchronous with the radius and, in turn, the electronegativity of the halogens (Figure SI-12). Investigations with respect to the σ_m constants,²¹ which would seem to be relevant considering the potential effect on the *meta*-nitrogen as a hydrogen acceptor, show very close electron withdrawing constants across all halogens.

In comparison to racemic SynVesT-1, only the larger halogen substituents in place of the pyridinyl 3-methyl compete in affinity (I (12b), 5.1 nM; Br (12c), 5.7 nM). With respect to electronic influences on the pyridinyl ring, methyl shows only a slightly donating σ_m value ($\sigma_m = -0.07$), but it is comparable to these halogens in surface area²² (Figure 3), which could play a role in potency. Finally, the results of the chloro and fluoro analogs when compared to racemic SynVesT-1 show a reduction in affinity. An interesting comparison is the 3-fluoropyridinyl

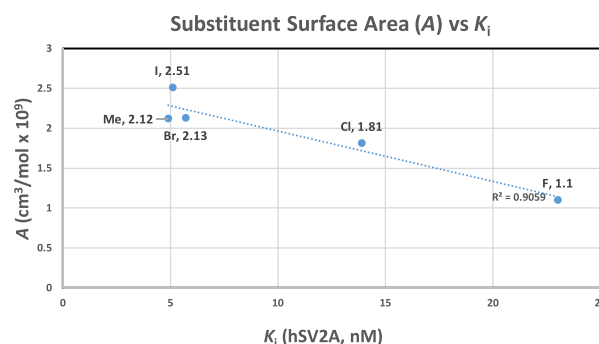


Figure 3. Relationship of the pyridinyl substituent surface area with potency.

analog of this series (3,5-difluorophenyl) with the 3,4,5-trifluorophenyl series. The 3,4,5-trifluorophenyl series shows a much less pronounced decrease in affinity when substituting the 3-methyl pyridinyl with fluorine, i.e., between racemic UCB-J (5.4 nM) and racemic UCB-H (12.0 nM).¹⁶

Ullrich²³ investigated the *N*-oxidation of pyridine and related compounds using *Agrocybe aegerita* peroxidase/ peroxygenase (AaP), a fungal enzyme that has been found to efficiently and selectively transfer oxygen to naphthalene and other aromatic substrates. AaP oxidized the pyridinyl nitrogen in the presence of H₂O₂ in 100% yield taking into account volatilized pyridine, which accounted for a 14% loss of the starting material (e.g., 86% yield, 100% relative conversion). One part of this study showed that pyridine derivatives substituted at the *meta*-position by different halogens were oxidized at the nitrogen in decreasing yields as the electronegativity of the halogen increased: I (102%), Br (62%), Cl (47%), and F (39%). These results support a trend demonstrating loss of electron density at pyridine/nitrogen (less readily oxidized) with increasing electronegativity of the halogen and, in turn, a decrease in potency. This helps support a hypothesis where decreased hydrogen bonding ability occurs as the electron withdrawing potential of the halogen increases.

2.4. Supporting Trends across all Compounds.

2.4.1. Surface Area of Substituents at the 3-Position of the Pyridinylmethyl Moiety. One observed trend across all of the above compounds is the surface area (*A*) of the bound moieties at the 3-position of the pyridinyl group.²² When using 3-methyl as a reference ($A = 2.12 \text{ cm}^3/\text{mol} \times 10^9$), the highest potencies are observed with compounds closest to this surface area (e.g., I and Br). This trend shows less sensitivity across the hydrocarbons than with halogens where the potency drops off more rapidly with deviation from this surface area (Figure SI-13).

2.4.2. Bioisosteric Equivalence and the Potential for Additional Hydrogen Bonding. Considering all the compounds reported here, the (3-ethynylpyridin-4-yl)methyl derivative (12a, 4.8 nM) showed the highest SV2A affinity and was virtually equivalent to our lead compound racemic SynVesT-1 (18, 4.9 nM) in potency. Bioisosteric equivalents of the ethynyl moiety are known and several of those (I, Br, and ethenyl) have been utilized in this work.²⁴ Our data demonstrates a bioisosteric relationship across our SAR study, and this relationship is most pronounced when comparing the 3-ethynyl, ethenyl, Br, and I substitutions (Table 1). One hypothesis with respect to all of these isosteres is their potential to act as a hydrogen donor or the equivalent and can interact with a hydrogen bond acceptor.^{24–26}

Although further investigation would be necessary to provide more detailed insights, it seems reasonable to say that although similar affinities are observed between the halogens and the hydrocarbons, these similar affinities could be related to a different balance between bonding interactions at the pyridinyl 3-position and pyridine nitrogen. One example derived from computer modeling studies suggests the nitrogen in 3-iodopyridine withdraws electron density from the iodine and increases its sigma-hole, thus making it more accessible for hydrogen bonding.²⁵ In this model that involves computer generated electrostatic potentials, 3-iodopyridine exhibits a donor–acceptor motif with iodine acting as a donor and the pyridine nitrogen as an acceptor. Although the 3-ethynyl pyridinyl model may resemble this to some extent, it could have significantly different electronic properties yet still result in

similar potency through a different donor–acceptor balance. π interactions might also be considered.²⁶

2.5. Potential Applications in PET/SPECT Imaging. The iodine analog (12b, 5.1 nM) could be radiolabeled with beta, gamma ray, and positron-emitting isotopes for autoradiography, SPECT, and PET imaging, respectively.

Radionuclides of iodine are widely used in nuclear medicine. Some applications include labeling of receptors, monoclonal antibodies, proteins, etc. These diagnostic and therapeutic applications require quantitative imaging that may extend for several days. ¹³¹I is often used for therapy due to its beta emission (606 keV) and emits gamma photons that can be used in SPECT imaging. ¹²³I is suitable for SPECT imaging with a gamma emission peak of 159 keV. This peak emission is close to that of ^{99m}Tc (140 keV) for which most SPECT camera design has been optimized. It has a relatively short half-life (13.22 h), which is favorable for the study of short metabolic processes. ¹²⁴I is attracting increasing interest for long-term clinical and PET studies. ¹²⁴I is a positron-emitting nuclide with a half-life of 4.2 days, and about 23% of disintegrations result in high energy positron emissions.^{27,28} Due to the optimal energy of emitted electrons, ¹²⁵I is commonly used in autoradiographic studies.²⁹ Thus, further *in vitro* and *in vivo* characterization of this SV2A ligand as a nuclear imaging agent is warranted.

3. CONCLUSIONS

A potent series of SV2A ligands has been discovered based on the racemic SynVesT-1 scaffold. Some of these analogs meet racemic SynVesT-1 in SV2A affinity, and several trends have been observed when comparing affinity against substituent properties in an effort to gain further insights into a previously published hydrogen bonding model. Linear potency trends are evident for the 3-halo pyridinyls with respect to the surface area, van der Waals radius, and electronegativity. Hammett constants (σ_m) are virtually equivalent across the halogens and do not show a linear relationship with affinity. Hydrocarbons show highly linear trends when comparing surface areas or Hammett constants against affinity. The 3-alkynyl pyridinyl derivative showed the highest affinity and affinity decreased across the hydrocarbons as hybridization increased. Affinity loss was observed when the pyridinyl nitrogen of racemic SynVesT-1 was moved to neighboring positions on the ring or oxidized, possibly indicating an influence on hydrogen bonding.

A bioisosteric trend appears to exist across the alkynyl, alkenyl, iodo, and bromo analogs, leaving opportunities for SAR exploration, and we envision an opportunity for additional bonding of these analogs at the 3-position of pyridinyl through sigma-hole bonding of the halogens or the alkynyl hydrogen. It remains unclear exactly which similarities across these new analogs are responsible for their comparable SV2A affinity to racemic SynVesT-1, which leaves much room for further exploration.

4. EXPERIMENTAL SECTION

4.1. General Chemistry Information. All reagents and solvents were obtained from commercial sources and used without further purification unless noted otherwise. Nuclear magnetic resonance (¹H) spectra were recorded on an Agilent DD2 400 MHz (A400a or c) NMR spectrometer. Chemical shifts are reported in parts per million, with the solvent resonance as the internal standard (CDCl₃: 7.26 ppm; DMSO-*d*₆: 2.50 ppm). The following abbreviations are used to denote

signal patterns: s = singlet, d = doublet, t = triplet, m = multiplet, and br = broad. High-resolution mass spectrometry (HRMS) was performed on a Thermo Scientific (Waltham, MA) LTQ Orbitrap ELITE mass spectrometer. Unless otherwise noted, flash chromatography was conducted by utilizing the Isolera Prime flash purification system from Biotage Inc. and SiliCycle, SliiaSep disposable normal-phase silica gel flash columns (4–120 g). Thin-layer chromatography was performed using 2.5 cm × 7.5 cm glass-backed TLC silica gel 60 F254 plates from EMD Millipore corporation (HX84750394) and visualized by UV light. The purity of all exemplified compounds was ≥95%, as determined by HPLC analysis and ¹H NMR.

4.1.1. (3-Ethynylpyridin-4-yl)methyl Methanesulfonate (11a). To a solution containing (3-ethynylpyridin-4-yl)methanol (**22**, 53 mg, 0.398 mmol), TEA (222 μL, 1.592 mmol), and DCM (4 mL) was added methanesulfonyl chloride (34.1 μL, 0.438 mmol) dropwise at rt. The solution was maintained for 1 h, diluted with DCM (15 mL), and washed with saturated sodium bicarbonate (10 mL). The organic portion was dried over sodium sulfate, filtered, and concentrated to a black residue. Purification on silica gel (0–70% EtOAc/Hex) afforded (3-ethynylpyridin-4-yl)methyl methanesulfonate (**11a**, 30 mg, 36%) as a clear residue that quickly turned purple red. The product was used immediately in the reaction leading to **12a** by diluting in THF and transferring.

4.1.2. (3-Iodopyridin-4-yl)methyl Methanesulfonate (11b). To a solution containing (3-iodopyridin-4-yl)methanol (**20**, 100 mg, 0.425 mmol), TEA (237 μL, 1.702 mmol), and DCM (2.4 mL) was added methanesulfonyl chloride (36.5 μL, 0.468 mmol) dropwise at rt. The solution was maintained for 1 h. The solution was concentrated to about 1.5 mL and loaded directly on to a 25 g silica gel flash column pre-equilibrated with hexanes. The product was eluted using 0–70% EtOAc/Hex. The combined fractions containing (3-iodopyridin-4-yl)methyl methanesulfonate (**11b**) were concentrated to approximately 2 mL volume and used immediately as a solution in the reaction leading to **12b**.

4.1.3. (3-Vinylpyridin-4-yl)methyl Methanesulfonate (11d). To a solution containing (3-vinylpyridin-4-yl)methanol (**23**, 100 mg, 0.740 mmol), TEA (309 μL, 2.22 mmol), and DCM (6 mL) was added methanesulfonyl chloride (63.4 μL, 0.814 mmol) dropwise at rt. The solution was maintained for 1 h, diluted with DCM (20 mL), and washed with saturated sodium bicarbonate (10 mL). The organic portion was dried over sodium sulfate and filtered. The solution was concentrated to about 2 mL and loaded on to a 25 g silica gel flash column pre-equilibrated with hexanes. The product was eluted using 100% EtOAc. The combined fractions containing (3-vinylpyridin-4-yl)methyl methanesulfonate (**11d**) were concentrated to approximately 2 mL volume and used immediately as a solution in the reaction leading to **12d**.

4.1.4. 4-(3,5-Difluorophenyl)-1-((3-ethynylpyridin-4-yl)methyl)pyrrolidin-2-one (12a). Compound **12a** was prepared as described for **12b** using 4-(3,5-difluorophenyl)pyrrolidin-2-one (**10**, 50 mg, 0.254 mmol), sodium hydride (15.21 mg, 0.380 mmol, 60%), tetrabutylammonium iodide (4.68 mg, 0.013 mmol), and (3-ethynylpyridin-4-yl)methyl methanesulfonate (**11a**, 30 mg, 0.142 mmol). Purification using silica gel flash chromatography (EtOAc/EtOH 0–10%) afforded 4-(3,5-difluorophenyl)-1-((3-ethynylpyridin-4-yl)methyl)pyrrolidin-2-one (**12a**, 24 mg, 30%) as a brown residue. ¹H NMR (400 MHz, CDCl₃) δ: 8.72 (s, 1H), 8.54 (d, J = 5.1 Hz, 1H), 7.22 (d, J = 5.1 Hz, 1H), 6.77–6.63 (m, 3H), 4.82–4.57 (m, 2H), 3.69

(dd, J = 9.7, 8.2 Hz, 1H), 3.64–3.53 (m, 1H), 3.47 (s, 1H), 3.30 (dd, J = 9.7, 6.8 Hz, 1H), 2.90 (dd, J = 17.0, 8.9 Hz, 1H), 2.58 (dd, J = 17.0, 8.2 Hz, 1H). HRMS calcd for C₁₈H₁₄F₂N₂O (M + H)⁺, 313.1147, found 313.1151.

4.1.5. 4-(3,5-Difluorophenyl)-1-((3-iodopyridin-4-yl)methyl)pyrrolidin-2-one (12b). To a solution containing 4-(3,5-difluorophenyl)pyrrolidin-2-one (**10**, 50 mg, 0.254 mmol) and THF (1.7 mL), cooled to 0 °C, was added sodium hydride (15.21 mg, 0.380 mmol, 60%) in one portion (gas evolution). The light tan mixture was removed from cooling and allowed to stir at ambient temperature for 1 h. A solution (~2 mL) containing (3-iodopyridin-4-yl)methyl methanesulfonate (**11b**, approximately 133 mg, 0.425 mmol) in EtOAc/Hex was added followed by tetrabutylammonium iodide (4.68 mg, 0.013 mmol). The light tan mixture was allowed to stir at rt. After 18 h, the reaction was quenched with two drops of water, concentrated to about half volume and directly loaded on to a 25 g silica gel flash column pre-equilibrated with EtOAc. The product was eluted with EtOAc/EtOH 0–10%. This afforded 4-(3,5-difluorophenyl)-1-((3-iodopyridin-4-yl)methyl)pyrrolidin-2-one (**12b**, 51 mg, 49%) as a dark purple residue. ¹H NMR (400 MHz, CDCl₃) δ: 8.92 (s, 1H), 8.49 (d, J = 5.0 Hz, 1H), 7.16 (d, J = 4.9 Hz, 1H), 6.72 (ddd, J = 11.8, 6.5, 2.1 Hz, 3H), 4.70–4.40 (m, 2H), 3.71 (dd, J = 9.4, 8.2 Hz, 1H), 3.68–3.57 (m, 1H), 3.32 (dd, J = 9.4, 6.8 Hz, 1H), 2.92 (dd, J = 17.0, 8.8 Hz, 1H), 2.61 (dd, J = 17.0, 8.3 Hz, 1H). HRMS calcd for C₁₆H₁₃F₂N₂O (M + H)⁺, 415.0113, found 415.0117.

4.1.6. 1-((3-Bromopyridin-4-yl)methyl)-4-(3,5-difluorophenyl)pyrrolidin-2-one (12c). Compound **12c** was prepared as described for **12e** using 4-(3,5-difluorophenyl)pyrrolidin-2-one (**10**, 75 mg, 0.380 mmol), sodium hydride (22.82 mg, 0.571 mmol, 60%), 3-bromo-4-(chloromethyl)pyridine hydrochloride (**11c**, 111 mg, 0.456 mmol), and tetrabutylammonium iodide (7.02 mg, 0.019 mmol). Purification using silica gel flash chromatography (EtOAc/EtOH 0–10%) afforded 1-((3-bromopyridin-4-yl)methyl)-4-(3,5-difluorophenyl)pyrrolidin-2-one (**12c**, 10 mg, 7%) as a purple/tan residue. ¹H NMR (400 MHz, CDCl₃) δ: 8.70 (s, 1H), 8.48 (d, J = 4.9 Hz, 1H), 7.17 (d, J = 5.0 Hz, 1H), 6.77–6.64 (m, 3H), 4.73–4.48 (m, 2H), 3.70 (dd, J = 9.6, 8.2 Hz, 1H), 3.60 (p, J = 8.2 Hz, 1H), 3.31 (dd, J = 9.5, 6.9 Hz, 1H), 2.89 (dd, J = 17.0, 8.9 Hz, 1H), 2.58 (dd, J = 17.0, 8.3 Hz, 1H). HRMS calcd for C₁₆H₁₃BrF₂N₂O (M + H)⁺, 367.0252, found 367.0259.

4.1.7. 4-(3,5-Difluorophenyl)-1-((3-vinylpyridin-4-yl)methyl)pyrrolidin-2-one (12d). Compound **12d** was prepared as described for **12b** using 4-(3,5-difluorophenyl)pyrrolidin-2-one (**10**, 75 mg, 0.380 mmol), sodium hydride (22.82 mg, 0.571 mmol, 60%), (3-vinylpyridin-4-yl)methyl methanesulfonate (**11d**, approximately 158 mg, 0.741 mmol), and tetrabutylammonium iodide (7.02 mg, 0.019 mmol). Purification using silica gel flash chromatography (EtOAc/EtOH 0–10%) afforded 4-(3,5-difluorophenyl)-1-((3-vinylpyridin-4-yl)methyl)pyrrolidin-2-one (**12d**, 40 mg, 34%) as a brown oil. ¹H NMR (400 MHz, CDCl₃) δ: 8.71 (s, 1H), 8.48 (d, J = 5.0 Hz, 1H), 7.11 (d, J = 5.0 Hz, 1H), 6.90 (dd, J = 17.4, 11.1 Hz, 1H), 6.75–6.60 (m, 3H), 5.75 (dd, J = 17.4, 1.1 Hz, 1H), 5.49 (dd, J = 11.1, 1.1 Hz, 1H), 4.69–4.48 (m, 2H), 3.54 (td, J = 7.8, 7.4, 3.4 Hz, 2H), 3.15 (q, J = 2.4 Hz, 1H), 2.97–2.82 (m, 1H), 2.62–2.45 (m, 1H). HRMS calcd for C₁₈H₁₆F₂N₂O (M + H)⁺, 315.1303, found 315.1304.

4.1.8. 4-(3,5-Difluorophenyl)-1-(pyridin-4-ylmethyl)pyrrolidin-2-one (12e). To a solution containing 4-(3,5-difluorophenyl)pyrrolidin-2-one (**10**, 75 mg, 0.380 mmol) and

THF (2.5 mL), cooled to 0 °C, was added sodium hydride (38.0 mg, 0.951 mmol, 60%) in one portion (gas evolution). The mixture was removed from cooling and allowed to stir at ambient temperature for 1 h. 4-(Chloromethyl)pyridine hydrochloride (**11e**, 68.6 mg, 0.418 mmol) was added followed by tetrabutylammonium iodide (7.02 mg, 0.019 mmol). The mixture was allowed to stir for 18 h, carefully added to saturated NaHCO₃ (15 mL), and the resultant aqueous solution was extracted with EtOAc (2 × 15 mL). The combined organic portions were washed with brine (15 mL), dried over sodium sulfate, filtered, and concentrated. Purification using silica gel flash chromatography (EtOAc/EtOH 0–10%) afforded 4-(3,5-difluorophenyl)-1-(pyridin-4-ylmethyl)pyrrolidin-2-one (**12e**, 30 mg, 27%) as a purple residue. ¹H NMR (400 MHz, CDCl₃) δ: 8.64–8.52 (m, 2H), 7.22–7.11 (m, 2H), 6.70 (td, *J* = 6.1, 5.5, 2.7 Hz, 3H), 4.63–4.37 (m, 2H), 3.70–3.49 (m, 2H), 3.27 (dd, *J* = 9.3, 6.5 Hz, 1H), 2.91 (dd, *J* = 17.0, 8.8 Hz, 1H), 2.59 (dd, *J* = 17.0, 8.0 Hz, 1H). HRMS calcd for C₁₆H₁₄F₂N₂O (M + H)⁺, 289.1147, found 289.1141.

4.1.9. 4-(3,5-Difluorophenyl)-1-((3-ethylpyridin-4-yl)methyl)pyrrolidin-2-one (12f). To a degassed solution containing 4-(3,5-difluorophenyl)-1-((3-ethynylpyridin-4-yl)methyl)pyrrolidin-2-one (**12a**, 50 mg, 0.160 mmol) and EtOAc (1.6 mL) was added palladium on carbon (10%, 8.52 mg, 8.00 μmol). The mixture was stirred quickly for 90 min at rt under an H₂ balloon. The reaction was filtered through celite (500 mesh, fine, acid washed) and the Pd/C was rinsed thoroughly with EtOAc on the Celite. The filtered solution/washes were concentrated to afford 4-(3,5-difluorophenyl)-1-((3-ethylpyridin-4-yl)methyl)pyrrolidin-2-one (**12f**, 50 mg, 99%) as a clear, oily residue. ¹H NMR (400 MHz, CDCl₃) δ: 8.50–8.38 (m, 2H), 7.06 (d, *J* = 5.0 Hz, 1H), 6.70 (pd, *J* = 4.2, 1.9 Hz, 3H), 4.56 (dd, *J* = 89.5, 15.4 Hz, 2H), 3.66–3.51 (m, 2H), 3.29–3.18 (m, 1H), 2.98–2.85 (m, 1H), 2.70 (q, *J* = 7.6 Hz, 2H), 2.66–2.54 (m, 1H), 1.25 (td, *J* = 7.4, 2.1 Hz, 3H). HRMS calcd for C₁₈H₁₈F₂N₂O (M + H)⁺, 317.1460, found 317.1457.

4.1.10. 1-((3-Chloropyridin-4-yl)methyl)-4-(3,5-difluorophenyl)pyrrolidin-2-one (12g). Compound **12g** was prepared as described for **12e** using 4-(3,5-difluorophenyl)pyrrolidin-2-one (**10**, 50 mg, 0.254 mmol), sodium hydride (15 mg, 0.380 mmol, 60%), 4-(bromomethyl)-3-chloropyridine hydrobromide (**11g**, 87 mg, 0.304 mmol), and tetrabutylammonium iodide (4.7 mg, 0.013 mmol). Purification using silica gel flash chromatography (EtOAc/EtOH 0–10%) afforded 1-((3-chloropyridin-4-yl)methyl)-4-(3,5-difluorophenyl)pyrrolidin-2-one (**12g**, 4 mg, 5%) as a clear residue. ¹H NMR (400 MHz, CDCl₃) δ: 8.58 (d, *J* = 11.2 Hz, 1H), 8.46 (dd, *J* = 16.1, 5.0 Hz, 1H), 7.21 (d, *J* = 4.9 Hz, 1H), 6.78–6.65 (m, 3H), 4.77–4.52 (m, 2H), 3.72 (dd, *J* = 9.6, 8.2 Hz, 1H), 3.67–3.55 (m, 1H), 3.32 (dd, *J* = 9.5, 6.9 Hz, 1H), 2.91 (dd, *J* = 17.0, 8.9 Hz, 1H), 2.60 (dd, *J* = 17.0, 8.3 Hz, 1H). HRMS calcd for C₁₆H₁₃ClF₂N₂O (M + H)⁺, 323.0757, found 323.0761.

4.1.11. 4-(3,5-Difluorophenyl)-1-((3-fluoropyridin-4-yl)methyl)pyrrolidin-2-one (12h). Compound **12h** was prepared as described for **12e** using 4-(3,5-difluorophenyl)pyrrolidin-2-one (**10**, 50 mg, 0.254 mmol), sodium hydride (15 mg, 0.380 mmol, 60%), 4-(chloromethyl)-3-fluoropyridine hydrochloride (**11h**, 55 mg, 0.304 mmol), and tetrabutylammonium iodide (4.7 mg, 0.013 mmol). Purification using silica gel flash chromatography (EtOAc/EtOH 0–10%) afforded 4-(3,5-difluorophenyl)-1-((3-fluoropyridin-4-yl)methyl)pyrrolidin-2-one (**12h**, 25 mg, 32%) as a purple/tan residue. ¹H NMR (400

MHz, CDCl₃) δ: 8.47 (s, 1H), 8.41 (d, *J* = 4.8 Hz, 1H), 7.32–7.21 (m, 1H), 6.71 (dd, *J* = 6.7, 3.2 Hz, 3H), 4.60 (q, *J* = 15.4 Hz, 2H), 3.80–3.66 (m, 1H), 3.59 (p, *J* = 8.2 Hz, 1H), 3.32 (dd, *J* = 9.6, 6.9 Hz, 1H), 2.88 (dd, *J* = 17.0, 9.0 Hz, 1H), 2.56 (dd, *J* = 17.0, 8.2 Hz, 1H). HRMS calcd for C₁₆H₁₃F₃N₂O (M + H)⁺, 307.1053, found 307.1053.

4.1.12. 4-(3,5-Difluorophenyl)-1-((2-methylpyridin-3-yl)methyl)pyrrolidin-2-one (12i). Compound **12i** was prepared as described for **12e** using 4-(3,5-difluorophenyl)pyrrolidin-2-one (**10**, 50 mg, 0.253 mmol), sodium hydride (7.6 mg, 0.304 mmol, 95%), tetrabutylammonium iodide (4.8 mg, 0.013 mmol), and 3-(chloromethyl)-2-methylpyridine hydrochloride (**11i**, 52 mg, 0.278 mmol). The mixture was stirred at rt for 18 h. Purification using silica gel flash chromatography (EtOAc/Hex 90–100%) afforded 4-(3,5-difluorophenyl)-1-((2-methylpyridin-3-yl)methyl)pyrrolidin-2-one (**12i**, 51 mg, 71%). ¹H NMR (400 MHz, CDCl₃) δ: 2.54–2.58 (m, 4H), 2.87 (dd, *J* = 16.0 Hz, *J* = 7.6 Hz, 1H), 3.18 (dd, *J* = 5.5 Hz, *J* = 2.9 Hz, 1H), 3.50–3.60 (m, 2H), 4.42 (d, *J* = 15.0 Hz, 1H), 4.62 (d, *J* = 15.0 Hz, 1H), 6.65–6.68 (m, 3H), 7.08–7.13 (m, 1H), 7.44–7.46 (m, 1H), 8.41 (s, 1H). HRMS calcd for C₁₇H₁₆F₂N₂O (M + H)⁺, 303.1303, found 303.1303.

4.1.13. 4-(3,5-Difluorophenyl)-1-((4-methylpyridin-3-yl)methyl)pyrrolidin-2-one (12j). Compound **12j** was prepared as described for **12e** using 4-(3,5-difluorophenyl)pyrrolidin-2-one (**10**, 50 mg, 0.253 mmol), sodium hydride (7.6 mg, 0.304 mmol, 95%), tetrabutylammonium iodide (4.8 mg, 0.013 mmol), and 3-(bromomethyl)-4-methylpyridine hydro bromide (**11j**, 77 mg, 0.278 mmol). The mixture was stirred at rt for 18 h. Purification using silica gel flash chromatography (EtOAc/Hex 90–100%) afforded 4-(3,5-difluorophenyl)-1-((4-methylpyridin-3-yl)methyl)pyrrolidin-2-one (**12j**, 55 mg, 70%). ¹H NMR (400 MHz, CDCl₃) δ: 2.31 (s, 3H), 2.51 (dd, *J* = 17.0 Hz, *J* = 7.8 Hz, 1H), 2.83 (dd, *J* = 16.9 Hz, *J* = 8.7 Hz, 1H), 3.12–3.16 (m, 1H), 3.45–3.56 (m, 2H), 4.44 (d, *J* = 14.9 Hz, 1H), 4.59 (d, *J* = 14.9 Hz, 1H), 6.60–6.65 (m, 3H), 7.09 (d, *J* = 4.9 Hz, 1H), 8.33 (s, 1H), 8.37 (d, *J* = 4.9 Hz, 1H). HRMS calcd for C₁₇H₁₆F₂N₂O (M + H)⁺, 303.1303, found 303.1305.

4.1.14. 4-((4-(3,5-Difluorophenyl)-2-oxopyrrolidin-1-yl)methyl)-3-methylpyridine 1-oxide (12k). To a solution containing 4-(3,5-difluorophenyl)-1-((3-methylpyridin-4-yl)methyl)pyrrolidin-2-one (**18**, 25 mg, 0.083 mmol) and THF (0.83 mL) was added mCPBA (37.1 mg, 0.165 mmol) at rt in one portion. The solution was maintained for 3 h and added to saturated NaHCO₃ (15 mL). The resultant aqueous mixture was extracted with EtOAc (30 mL). The organic portion was washed with water (15 mL), washed with brine (15 mL), dried over Na₂SO₄, filtered, and concentrated to a white residue. Purification using silica gel flash chromatography (DCM/MeOH 0–10%) afforded 4-((4-(3,5-difluorophenyl)-2-oxopyrrolidin-1-yl)methyl)-3-methylpyridine 1-oxide (**12k**, 12 mg, 46%) as a white solid. ¹H NMR (400 MHz, CDCl₃) δ: 8.13–7.97 (m, 2H), 7.06 (d, *J* = 6.5 Hz, 1H), 6.77–6.61 (m, 3H), 4.64–4.30 (m, 2H), 3.61 (ddd, *J* = 14.7, 12.0, 7.5 Hz, 2H), 3.24 (dd, *J* = 8.8, 6.2 Hz, 1H), 2.89 (dd, *J* = 17.1, 8.7 Hz, 1H), 2.58 (dd, *J* = 17.0, 7.7 Hz, 1H), 2.28 (s, 3H). HRMS calcd for C₁₇H₁₆F₂N₂O₂ (M + H)⁺, 319.1253, found 319.1257.

4.1.15. 4-(3,5-Difluorophenyl)-1-((3-methylpyridin-4-yl)methyl)pyrrolidin-2-one (18, Racemic SynVesT-1). Compound **18** (racemic SynVesT-1) was prepared as described for **12e** using 4-(3,5-difluorophenyl)pyrrolidin-2-one (**10**, 100 mg, 0.507 mmol), sodium hydride (81 mg, 2.029 mmol, 60%), tetrabutylammonium iodide (18.7 mg, 0.051 mmol), and 4-

(chloromethyl)-3-methylpyridine hydrochloride (135 mg, 0.761 mmol). The mixture was stirred at 50 °C for 18 h. Purification using silica gel flash chromatography (EtOAc/EtOH 0–10%) afforded 4-(3,5-difluorophenyl)-1-((3-methylpyridin-4-yl)methyl)pyrrolidin-2-one (**18**, racemic SynVesT-1, 123 mg, 80%) as a light purple, oily residue that solidified on standing. ¹H NMR (400 MHz, CDCl₃) δ: 8.42 (d, *J* = 3.8 Hz, 2H), 7.04 (d, *J* = 4.9 Hz, 1H), 6.71 (tt, *J* = 5.4, 2.4 Hz, 3H), 4.68–4.35 (m, 2H), 3.68–3.52 (m, 2H), 3.24 (hept, *J* = 5.0, 4.4 Hz, 1H), 2.98–2.84 (m, 1H), 2.60 (dd, *J* = 17.0, 8.0 Hz, 1H), 2.31 (s, 3H).

4.2. Competition Radioligand Binding Assays. Competition radioligand binding assays were run twice independently using separate assay materials. Some compounds were run a second time through this paradigm and are marked with an “*n* = 2” in Table 1 and the Results and Discussion section. Compounds were dissolved in DMSO (Sigma-Aldrich) to a concentration of 10 mM. Each 10 mM DMSO stock was serially diluted in PBS at pH 7.4 (Gibco) with 0.1% BSA to give 12 half-log dilutions from 10 μM to 32 pM when added to the assay (20 μL of a 10X working stock). Fresh frozen human brain (normal donor) was obtained from ABS Bio (Wilmington, DE). Duplicate samples of frontal cortex gray matter were homogenized in PBS at a concentration of 10 mg wet weight per mL for storage at –80 °C and further diluted to 4 mg/mL in PBS on the day of the assays. The final membrane concentration in the assay was 0.4 mg/mL (100 μL of 2X working stock per 200 μL reaction). [³H]UCB-J was synthesized by rhodium-black mediated hydrogen/tritium exchange to a specific activity of 34.9 Ci/mmol and a radiochemical purity of 98.9% and diluted in duplicate to a concentration of 6.25 nM in PBS to give 2.5X working stocks (the final concentration in the plate was 2.5 nM). Working stocks of membranes (100 μL), blocking compounds (20 μL), and radioligand (80 μL) were combined in quadruplicate wells of 96-well plates, sealed, and incubated at room temperature on an orbital shaker at 250 RPM for 90 min to achieve binding equilibrium. Reaction plates were filtered onto Multiscreen GF/B Harvest Plates (Millipore) and rapidly washed with 300 mL of cold PBS. The plates were allowed to dry, sealed on the bottom, and 40 μL of Microscint-20 scintillation cocktail (Perkin-Elmer) was added to all wells before affixing a clear top seal and counting using a Microbeta2 plate reader (Perkin-Elmer). Technical replicates (*n* = 4) from each independent assay were averaged in Microsoft Excel, and the duplicate values for each point were plotted and analyzed in GraphPad Prism using the built-in 1-site *K_i* model. The curve fitting provided *K_i* values and 95% confidence intervals used to compare compounds for statistical differences, indicated by nonoverlapping 95% confidence bands (Figure SI-14).

■ ASSOCIATED CONTENT

SI Supporting Information

The Supporting Information is available free of charge at <https://pubs.acs.org/doi/10.1021/acsomega.1c02433>.

NMR spectra (pages S2–S8), experimental details for intermediates leading to **11a**, **11b**, and **11d** (pages S8–S10), scatter plots related to observed potency trends (page S11 and S12), analytical HPLC chromatograms (pages S13–S16) (PDF)

■ AUTHOR INFORMATION

Corresponding Authors

Songye Li – PET Center, Yale University School of Medicine, New Haven, Connecticut 06520, United States; orcid.org/0000-0002-6096-8756; Email: songye.li@yale.edu

Zhengxin Cai – PET Center, Yale University School of Medicine, New Haven, Connecticut 06520, United States; orcid.org/0000-0002-2005-6760; Email: jason.cai@yale.edu

Authors

Richard Pracitto – PET Center, Yale University School of Medicine, New Haven, Connecticut 06520, United States; Present Address: Present address: Biohaven Labs, Biohaven Pharmaceuticals Inc., New Haven, Connecticut 06510, United States (R.P.)

Kyle C. Wilcox – Translational Imaging Neuroscience, AbbVie, North Chicago, Illinois 60064, United States

Marcel Lindemann – PET Center, Yale University School of Medicine, New Haven, Connecticut 06520, United States; Present Address: Present address: Nuclear Medicine and Radiation Biology Research Group, Department of Clinical Medicine, UiT The Arctic University of Norway, Tromsø, Norway (M.L.); Present Address: Present address: The PET Imaging Center, University Hospital of North Norway, Tromsø, Norway (M.L.)

Jie Tong – PET Center, Yale University School of Medicine, New Haven, Connecticut 06520, United States

Chao Zheng – PET Center, Yale University School of Medicine, New Haven, Connecticut 06520, United States; orcid.org/0000-0002-2179-8096

Sjoerd J. Finnema – PET Center, Yale University School of Medicine, New Haven, Connecticut 06520, United States; Translational Imaging Neuroscience, AbbVie, North Chicago, Illinois 60064, United States

Yiyun Huang – PET Center, Yale University School of Medicine, New Haven, Connecticut 06520, United States

Complete contact information is available at:

<https://pubs.acs.org/10.1021/acsomega.1c02433>

Author Contributions

The manuscript was written through contributions of all authors. All authors have given approval to the final version of the manuscript.

Notes

The authors declare no competing financial interest.

■ ACKNOWLEDGMENTS

This research was supported by NIH K01EB023312 and R01AG058773. Z.C. is an Archer Foundation Research Scientist.

■ ABBREVIATIONS

PET, positron emission tomography; SPECT, single-photon emission computed tomography; AD, Alzheimer's disease; PD, Parkinson's disease; SAR, structure–activity relationship

■ REFERENCES

(1) Cai, Z.; Li, S.; Matuskey, D.; Nabulsi, N.; Huang, Y. PET imaging of synaptic density: A new tool for investigation of neuropsychiatric diseases. *Neurosci. Lett.* **2019**, *691*, 44–50.

- (2) Takamori, S. Synaptic Vesicles. In *Encyclopedia of Neuroscience*; 2009; pp. 801–808, DOI: 10.1016/B978-008045046-9.01392-9.
- (3) Mercier, J.; Archen, L.; Bollu, V.; Carré, S.; Evrard, Y.; Jnoff, E.; Kenda, B.; Lallemand, B.; Michel, P.; Montel, F.; Moureau, F.; Price, N.; Quesnel, Y.; Sauvage, X.; Valade, A.; Provins, L. Discovery of heterocyclic nonacetamide synaptic vesicle protein 2A (SV2A) ligands with single-digit nanomolar potency: opening avenues towards the first SV2A positron emission tomography (PET) ligands. *Chem. Med. Chem.* **2014**, *9*, 693–698.
- (4) Finnema, S. J.; Nabulsi, N. B.; Eid, T.; Detyniecki, K.; Lin, S. F.; Chen, M. K.; Dhaher, R.; Matuskey, D.; Baum, E.; Holden, D.; Spencer, D. D.; Mercier, J.; Hannestad, J.; Huang, Y.; Carson, R. E. Imaging synaptic density in the living human brain. *Sci. Transl. Med.* **2016**, *8*, 348ra96.
- (5) Chen, M. K.; Mecca, A. P.; Naganawa, M.; Finnema, S. J.; Toyonaga, T.; Lin, S. F.; Najafzadeh, S.; Ropchan, J.; Lu, Y.; McDonald, J. W.; Michalak, H. R.; Nabulsi, N. B.; Arnsten, A. F. T.; Huang, Y.; Carson, R. E.; van Dyck, C. H. Assessing Synaptic Density in Alzheimer Disease With Synaptic Vesicle Glycoprotein 2A Positron Emission Tomographic Imaging. *JAMA Neurol.* **2018**, 1215.
- (6) Matuskey, D.; Tinaz, S.; Wilcox, K. C.; Naganawa, M.; Toyonaga, T.; Dias, M.; Henry, S.; Pittman, B.; Ropchan, J.; Nabulsi, N.; Suridjan, I.; Comley, R. A.; Huang, Y.; Finnema, S. J.; Carson, R. E. Synaptic Changes in Parkinson Disease Assessed with in vivo Imaging. *Ann. Neurol.* **2020**, *87*, 329–338.
- (7) Holmes, S. E.; Scheinost, D.; Finnema, S. J.; Naganawa, M.; Davis, M. T.; DellaGioia, N.; Nabulsi, N.; Matuskey, D.; Angarita, G. A.; Pietrzak, R. H.; Duman, R. S.; Sanacora, G.; Krystal, J. H.; Carson, R. E.; Esterlis, I. Lower synaptic density is associated with depression severity and network alterations. *Nat. Commun.* **2019**, *10*, 1529.
- (8) Onwordi, E. C.; Half, E. F.; Whitehurst, T.; Mansur, A.; Cotel, M.-C.; Wells, L.; Creaney, H.; Bonsall, D.; Rogdaki, M.; Shatalina, E.; Reis Marques, T.; Rabiner, E. A.; Gunn, R. N.; Natesan, S.; Vernon, A. C.; Howes, O. D. Synaptic density marker SV2A is reduced in schizophrenia patients and unaffected by antipsychotics in rats. *Nat. Commun.* **2020**, *11*, 246.
- (9) Nabulsi, N.; Mercier, J.; Holden, D.; Carre, S.; Najafzadeh, S.; Vandergeten, M.-C.; Lin, S.-f.; Deo, A. K.; Price, N.; Wood, M.; Lara-Jaime, T.; Montel, F.; Laruelle, M.; Carson, R. E.; Hannestad, J.; Huang, Y. Synthesis and Preclinical Evaluation of ¹¹C-UCB-J as a PET Tracer for Imaging the Synaptic Vesicle Glycoprotein 2A in the Brain. *J. Nucl. Med.* **2016**, 777.
- (10) Estrada, S.; Lubberink, M.; Thibblin, A.; Sprycha, M.; Buchanan, T.; Mestdagh, N.; Kenda, B.; Mercier, J.; Provins, L.; Gillard, M.; Tytgat, D.; Antoni, G. [¹¹C]UCB-A, a novel PET tracer for synaptic vesicle protein 2A. *Nucl. Med. Biol.* **2016**, *43*, 325–332.
- (11) Bastin, C.; Bahri, M. A.; Meyer, F.; Manard, M.; Delhay, E.; Plenevaux, A.; Becker, G.; Seret, A.; Mella, C.; Giacomelli, F.; Degueldre, C.; Balteau, E.; Luxen, A.; Salmon, E. In vivo imaging of synaptic loss in Alzheimer's disease with [¹⁸F]UCB-H positron emission tomography. *Eur. J. Nucl. Med. Mol. Imaging* **2020**, *47*, 390–402.
- (12) Warnock, G. I.; Aerts, J.; Bahri, M. A.; Bretin, F.; Lemaire, C.; Giacomelli, F.; Mievis, F.; Mestdagh, N.; Buchanan, T.; Valade, A.; Mercier, J.; Wood, M.; Gillard, M.; Seret, A.; Luxen, A.; Salmon, E.; Plenevaux, A. Evaluation of ¹⁸F-UCB-H as a novel PET tracer for synaptic vesicle protein 2A in the brain. *J. Nucl. Med.* **2014**, *55*, 1336–1341.
- (13) Li, S.; Cai, Z.; Wu, X.; Holden, D.; Praticto, R.; Kapinos, M.; Gao, H.; Labaree, D.; Nabulsi, N.; Carson, R. E.; Huang, Y. Synthesis and in Vivo Evaluation of a Novel PET Radiotracer for Imaging of Synaptic Vesicle Glycoprotein 2A (SV2A) in Nonhuman Primates. *ACS Chem. Neurosci.* **2019**, *10*, 1544–1554.
- (14) Cai, Z.; Li, S.; Zhang, W.; Praticto, R.; Wu, X.; Baum, E.; Finnema, S. J.; Holden, D.; Toyonaga, T.; Lin, S.-f.; Lindemann, M.; Shirali, A.; Labaree, D. C.; Ropchan, J.; Nabulsi, N.; Carson, R. E.; Huang, Y. Synthesis and Preclinical Evaluation of an ¹⁸F-Labeled Synaptic Vesicle Glycoprotein 2A PET Imaging Probe: [¹⁸F]SynVesT-2. *ACS Chem. Neurosci.* **2020**, *11*, 592–603.
- (15) Kenda, B. M.; Matagne, A. C.; Talaga, P. E.; Pasau, P. M.; Differding, E.; Lallemand, B. I.; Frycia, A. M.; Moureau, F. G.; Klitgaard, H. V.; Gillard, M. R.; Fuks, B.; Michel, P. Discovery of 4-Substituted Pyrrolidone Butanamides as New Agents with Significant Antiepileptic Activity. *J. Med. Chem.* **2004**, *47*, 530–549.
- (16) Patel, S.; Knight, A.; Krause, S.; Teceno, T.; Tresse, C.; Li, S.; Cai, Z.; Gouasmat, A.; Carroll, V. M.; Barret, O.; Gottmukkal, V.; Zhang, W.; Xiang, X.; Morley, T.; Huang, Y.; Passchier, J. Preclinical *In Vitro* and *In Vivo* Characterization of Synaptic Vesicle 2A-Targeting Compounds Amenable to F-18 Labeling as Potential PET Radioligands for Imaging of Synapse Integrity. *Mol. Imaging Biol.* **2020**, *22*, 832–841.
- (17) Abraham, M. H.; Honcharova, L.; Rocco, S. A.; Acree, W. E., Jr.; De Fina, K. M. The lipophilicity and hydrogen bond strength of pyridine-N-oxides and protonated pyridine-N-oxides. *New J. Chem.* **2011**, *35*, 930–936.
- (18) Becker, G.; Warnier, C.; Serrano, M. E.; Bahri, M. A.; Mercier, J.; Lemaire, C.; Salmon, E.; Luxen, A.; Plenevaux, A. Pharmacokinetic Characterization of [¹⁸F]UCB-H PET Radiopharmaceutical in the Rat Brain. *Mol. Pharmaceutics* **2017**, *14*, 2719–2725.
- (19) Lukomska, M.; Rybarczyk-Pirek, A. J.; Jabłoński, M.; Palusiak, M. The nature of NO-bonding in N-oxide group. *Phys. Chem. Chem. Phys.* **2015**, *17*, 16375–16387.
- (20) Balevicius, V.; Aidas, K.; Svoboda, I.; Fuess, H. Hydrogen bonding in pyridine N-oxide/acid systems: proton transfer and fine details revealed by FTIR, NMR, and X-ray diffraction. *J. Phys. Chem. A* **2012**, *116*, 8753–8761.
- (21) Hansch, C.; Leo, A.; Taft, R. W. A Survey of Hammett Substituent Constants and Resonance and Field Parameters. *Chem. Rev.* **1991**, *91*, 165–195.
- (22) Bondi, A. van der Waals Volumes and Radii. *J. Phys. Chem.* **1964**, *68*, 441–451.
- (23) Ullrich, R.; Dolge, C.; Kluge, M.; Hofrichter, M. Pyridine as novel substrate for regioselective oxygenation with aromatic peroxygenase from *Agroclybe aegerita*. *FEBS Lett.* **2008**, *582*, 4100–4106.
- (24) Talele, T. T. Acetylene Group, Friend or Foe in Medicinal Chemistry. *J. Med. Chem.* **2020**, *63*, 5625–5663.
- (25) Wilcken, R.; Zimmermann, M. O.; Lange, A.; Joerger, A. C.; Boeckler, F. M. Principles and applications of halogen bonding in medicinal chemistry and chemical biology. *J. Med. Chem.* **2013**, *56*, 1363–1388.
- (26) Wang, H.; Wang, W.; Jin, W. J. σ -Hole Bond vs π -Hole Bond: A Comparison Based on Halogen Bond. *Chem. Rev.* **2016**, *116*, 5072–5104.
- (27) Cascini, G. L.; Niccoli Asabella, A.; Notaristefano, A.; Restuccia, A.; Ferrari, C.; Rubini, D.; Altini, C.; Rubini, G. ¹²⁴Iodine: a longer-life positron emitter isotope-new opportunities in molecular imaging. *Biomed. Res. Int.* **2014**, *2014*, 672094.
- (28) Kukur, R.; Szejnberg, M.; Gulec, S. I-124 Imaging and Dosimetry. *Mol. Imaging. Radionucl. Ther.* **2017**, *26*, 66–73.
- (29) Wellendorph, P.; Hög, S.; Sabbatini, P.; Pedersen, M. H. F.; Martiny, L.; Knudsen, G. M.; Frølund, B.; Clausen, R. P.; Bräuner-Osborne, H. Novel radioiodinated γ -hydroxybutyric acid analogues for radiolabeling and Photolinking of high-affinity γ -hydroxybutyric acid binding sites. *J. Pharmacol. Exp. Ther.* **2010**, *335*, 458–464.

NOTE ADDED AFTER ASAP PUBLICATION

This paper was published ASAP on October 8, 2021 with an error in the references. The error was corrected, and the revised paper reposted on October 11, 2021.